International Journal of Energy
ISSN: 2957-9473 | Vol. 2, No. 1, 2023

Solar cell defect detection based on improved G-SSD Network

Mingyang Xu*

School of Electrical and Information Engineering, Northeast Petroleum University, Daqing, China
* **Corresponding author**: Email: 15049904033@163.com

Abstract: Aiming at the problems of finger interruptions, microcracks and shadow defects of solar cells that are not easy to detect and will reduce the efficiency of the cells, a solar cell defect localization detection algorithm based on improved G-SSD network is proposed. For object detection algorithms, the detection of small targets is challenging. Firstly, the input scale and network model are improved for the detection of small-scale targets. Secondly, in order to reduce the weight of the network model, a more lightweight network GhostNet is selected instead of VGG-16 in the experiment to reduce the computational cost of the network model. Finally, the EL image is input into the network for classification and positioning, and the prediction results are integrated and the final detection results are output. Experimental results show that compared with the original model, the mean (mAP) of the improved G-SSD is increased by 0.68%, effectively reduces some computing costs.

Keywords: Solar cell defect detection; G-SSD Network.

1. Introduction

Under the background of 'dual carbon', countries have vigorously developed clean energy such as photovoltaic, wind power, nuclear power, and hydropower to gradually replace fossil energy power generation, and at the same time, due to the cost advantage of photovoltaic power generation, it is favored by all countries. However, as PV energy systems reach terawatts, even a slight degradation in solar cell performance could lead to a loss of thousands of GWh of annual global power generation. PV modules will inevitably produce certain defects in the process of production, transportation and installation, resulting in great economic losses and even fires. Therefore, the defect detection of photovoltaic modules is highly valued.

The defect detection methods of photovoltaic modules can be divided into four types according to their detection principles: ultrasonic resonance scanning, contact resistance scanning, photoluminescence (PL) detection and electroluminescence (EL) detection. Although the sensitivity of ultrasonic detection method is not very high, it can be used for silicon wafers and cells due to its non-destructive and fast characteristics [1]; Although the contact resistance scanning method is highly sensitive, it is time-consuming and destructive, and is only suitable for cells [2]; Photoluminescence [3] and electroluminescence [4], although they need to filter out visible light, but they have the advantages of fast, online detection and high sensitivity, among which photoluminescence method is suitable for silicon wafers and cells, and electroluminescence method is suitable for cells and components. Considering the fast and efficient requirements of the production line, electroluminescence detection is more suitable. At present, most of the testing relies on manual labor, which must have many insurmountable problems, such as difficult unification of standards, misjudgment and missed detection, etc., which will have a negative impact on the efficiency of solar power generation systems.

In recent years, with the continuous update of deep learning networks, they have been more and more widely used in the defect detection of photovoltaic modules. Liu Anyi et al. [5] designed a localization detection algorithm for crack defects of solar cells obtained by photoluminescence, and proposed an improved U-net network algorithm, which has a recognition rate of 99.25% for crack defects, but the detection speed can continue to be enhanced. Tian Xiaojie et al. [6] used the proposed improved deep learning detection algorithm based on Yolov3 to locate and detect the crack defects of solar cells obtained by electroluminescence, and achieved 94% recognition accuracy, but the ability to detect irregular shapes needs to be improved.

Therefore, on the basis of the above research, the author uses the advantages of SSD algorithm and GhostNet network, different from the traditional network model, and proposes a solar cell defect localization detection algorithm based on improved SSD network, which is designed for the broken grid, crack and shadow defects of solar cells. Experimental results show that the proposed method has good feasibility and effectiveness.

2. Theoretical basis

2.1. SSD algorithm principle

The SSD model mainly includes a two-part network structure: first, the basic model adopts VGG-16, and uses Conv6 and Conv7 to replace the fully connected layer FC6 and FC7, while removing the dropout layer and FC8 layer, and adding 4 convolutional layers to obtain more feature maps for detection. At this point, a complete network model is built, and the network structure of the SSD is shown in Fig.

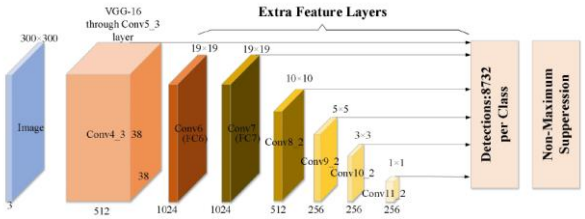


Figure 1. the network structure of the SSD.

It is obvious from the network structure that SSD use multi-

scale feature maps for detection. The six convolutional layers used to extract the feature map are Conv4_3, Conv7, Conv8_2, Conv9_2, Conv10_2, Conv11_2, and the size of the obtained feature map is (38×38), (19×19), (10×10), (5×5), (3×3), (1×1), and its size is reduced layer by layer, all for detection. Among them, the feature map with relatively small size is used to detect large targets, while the feature map with large size is used to detect relatively small targets, so as to achieve multi-scale target detection, and finally the final detection result is obtained through non-maximum suppression.

The SSD algorithm model has achieved good results in the accuracy and real-time of object detection, but there are also two problems. The first is that the accuracy of small-scale target detection is not high enough. Although the SSD algorithm adopts a pyramid-like structure in the detection process and designs and predicts multi-scale targets for each layer, there are still difficulties in detecting small-scale targets. The second is that the algorithm model has a high computational cost. The SSD algorithm uses VGG16 network as the basic network for feature extraction by default, but the feature extraction effect of VGG16 network is general, and the training cost and computing cost of the network are high, so it is difficult to achieve the purpose of lightweight.

2.2. The principle of the GhostNet algorithm

GhostNet uses fewer parameters than ordinary convolutional neural networks when generating feature maps. The motivation is to improve the redundancy of feature maps in neural networks. There is a certain degree of redundancy in the feature map in the neural network, and these redundant feature maps also enhance the network's ability to understand features to a certain extent, and these redundant feature maps are also essential for a successful model. GhostNet is a combination of multiple Ghost BottleNecks, which are stacked on top of two Ghost Modules.

2.2.1. Ghost Module principle.

Deep convolutional neural networks usually refer to convolutional neural networks composed of a large number of convolutions, and the commonly used convolution is shown in Fig. 2, and its computational amount (ignoring bias calculations) is approximately equal $h * w * c * n * w' * h'$, resulting in a large computational cost. Although recent studies such as MobileNet and ShuffleNet introduce deep convolution or shuffle operations to build efficient CNNs using smaller convolution kernels (floating-point arithmetic), the remaining convolutional layers will still take up a lot of memory and FLOPs.

The Ghost Module is divided into three steps: conventional convolution, Ghost generation and feature map stitching:

First, the eigenmap is obtained by conventional convolution, and the calculation amount is about $h * w * c * n * w' * h'$(for simplicity, ignore the bias term).

$$Y' = X * f' \quad (1)$$

where $f \in \mathbb{R}^{c \times k \times k \times m}$ is the convolution kernel used, m ≤ n.

Second, each original feature(Y') in the pair is processed by linear operation to generate the corresponding Ghost feature map(Yij):

$$y_{ij} = \Phi_{i,j}(y'_i), \forall i = 1, \cdots, s \quad (2)$$

where y'i is the Y'th original feature map.

Third, the obtained eigenmap and Ghost feature map are spliced to get the OutPut

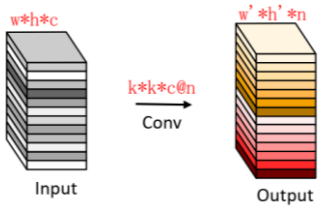


Figure 2. Regular convolution

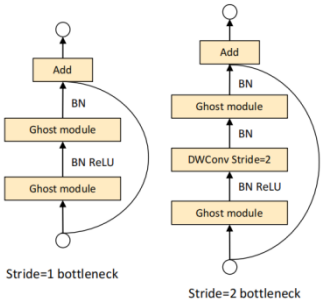


Figure 3. Ghost BottleNeck.

By using the Ghost module to generate a feature map consistent with the number of ordinary convolutional layers, the convolutional layers in the existing designed neural network structure can be replaced with the Ghost module to reduce the operation cost.

2.2.2. Ghost BottleNeck Principle.

The overall architecture of Ghost BottleNeck is very similar to Residual Block, as shown in Fig. 3, Ghost bottleneck is mainly composed of two stacked Ghost modules. The first Ghost module is used as an expansion layer, increasing the number of channels. The second Ghost module reduces the number of channels to match the shortcut path. Then, use Shortcut to connect the inputs and outputs of these two Ghost modules. The second Ghost module does not use ReLU after that, and the other layers apply batch normalization (BN) and ReLU nonlinear activation after each layer. The above Ghost bottleneck applies to stride=1, and in the case of stride=2, the shortcut path is implemented by the downsampling layer and the Depthwise Convolution of stride=2.

3. Improved G-SSD defect detection algorithm model

3.1. Feature extraction network improvements

Firstly, the feature extraction network of the SSD model is VGG-16, but the VGG-16 model is too large, which has the problem of large parameter cost and calculation cost. Secondly, SSD defect detection networks have certain defects for small target detection. Therefore, in order to further reduce the number of parameters of the model to improve the detection speed of the model, and overcome the disadvantages of small target detection, this chapter is improved in the following two aspects:

(1) The GhostNet model is selected instead of VGG-16 as the feature extraction network, and the first 16 layers of the structure are selected as the backbone to achieve the purpose of lightweight.

(2) Increase the network input scale, change the input from 300×300×3 to 320×320×3, select 40×40, 20×20, 10×10, 5×5, 3×3, 1×1 feature layer size, increase the picture input range, expand the prediction accuracy of the network, and improve the shortcomings of SSD algorithm for small target detection. Wang et al. [7] proved through experiments that when the

input image size is increased to 320, the mAP value is increased by 8.5% and 3.7% on the MS COCO and PASCAL VOC test sets, respectively, and the detection accuracy of small targets is greatly improved.

3.2. Secondary network layer improvements

According to the detection requirements, three convolutional layers, Conv_2, Conv_3 and Conv_4, are added after the G-bneck_16 of GhostNet for feature map extraction, and the following improvements are made to the auxiliary network layer to achieve the optimal detection effect according to the problems existing in the SSD model.

(1) G-bneck_6, G-bneck_12, G-bneck_16, Conv2_2, Conv3_2, and Conv4_2 are selected as convolutional layers for object detection. Select the default number of boxes for [4,6,6,6,4,4], resulting in 9620 default boxes, as shown in Table 1. By increasing the number of default frames, the purpose of increasing the accuracy of target detection is achieved.

Table 1. The default number of boxes for different feature layers.

Feature layer name	Feature layer dimensions	The number of a priori boxes	Total number of prior boxes
G-bneck_6	40*40	4	6400
G-bneck_12	20*20	6	2400
G-bneck_16	10*10	6	600
Con2_2	5*5	6	180
Con3_2	3*3	4	36
Con4_2	1*1	4	4

(2) The auxiliary network uses the Mish [8] activation function instead of the ReLU6 activation function.

The activation function Mish has a lower computational cost than the activation function swish, and replaces the sigmoid function in the calculation, eliminating the potential numerical accuracy loss caused by the sigmoid activation function when implemented in different situations. The accuracy of the activation function Mish proposed by [8] is 0.494% higher than Swish and 1.671% higher than that of ReLU, which is suitable for the second half of the model, so this chapter replaces the activation function of the deep network with Mish.

4. Experimental analysis

4.1. Dataset settings.

The experimental data used in this paper is a public dataset published by Buerhop-Lutz et al. [9], which provides images of solar cells extracted from high-resolution EL images of photovoltaic modules. In this paper, a total of 600 images of finger interruptions, microcracks and shadow defects detected by electroluminescence were collected as experimental datasets.

The EL test images of the three defect images of finger interruptions, microcracks and shadow are annotated, as shown in Fig. 4, and the image is annotated by using the annotation tool Label Image. After the annotation is completed, the VOC dataset is established. Since there is less experimental data in this chapter, the validation set is not set. In this experiment, a total of 600 images were annotated and used for experimental testing according to the ratio of 9:1 between the training set and the test set.

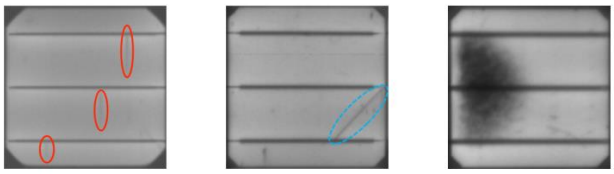


Figure 4. The three defect images of finger interruptions, microcracks and shadow.

4.2. Experimental results

In order to verify the superiority of the algorithm in this chapter, the algorithm in this chapter is experimentally compared with the SSD-VGG16 model and the SSD-Ghost model, and the results are shown in Table 2 and Table 3.

Table 2. Experimental Results.

Module	AP(%)			mAP (%)
	finger interruptions	microcrack	shadow	
SSD-VGG16	98.11%	97.96%	98.23%	98.1%
SSD-Ghost	98.36%	98.26%	98.47%	98.36%
Improved G-SSD	98.56%	98.75%	99.03%	98.78%

Table 3. Experiment Time results.

Module	SSD-VGG16	SSD-Ghost	Improved G-SSD
Fps	69	132	142

It can be seen from Table 2 that compared with SSD-VGG16 and SSD-Mobilenetv3 models, the improved G-SSD model proposed in this chapter achieves the highest average accuracy (AP) in finger interruptions, microcracks and shadow defects, with 98.56%, 98.75% and 99.03%, respectively. The overall mean (mAP) improved by 0.68% and 0.42%, respectively, the highest among the three. It is proved that the improved G-SSD has good detection and recognition effect for the broken grid, crack and shadow defects of solar cell EL test images, and compared with the improved model, the recognition accuracy is significantly improved, and the detection accuracy is high, and it has good applicability for the defect detection of solar cell EL test images.

Table 3 shows that the detection rate (Fps) is significantly improved by replacing the VGG16 network with the lightweight network GhostNet, which proves that the GhostNet network can alleviate the problems of large parameters and high computing cost of VGG16 network. Therefore, the G-SSD algorithm has good accuracy and timeliness in the detection of solar cell EL test image disgrating, cracking and shadow defect location.

5. Conclusion

Compared with other detection methods, the proposed method has higher feature extraction ability and fault recognition ability, and the experimental results show that it has important application value in the field of solar electroluminescence image defect recognition and detection. In addition, the method can also make more granular category differentiation, and due to the reduction of model parameters and the simplicity of the method, it also has a wide application prospect in micro-computing systems.

References

[1] S. Ostapenko, W. Dallas, D Hess, et al. Crack Detection and Analyses using Resonance Ultrasonic Vibrations in Crystalline Silicon Wafers; proceedings of the IEEE World Conference on Photovoltaic Energy Conversion, F, 2007 [C].

[2] D. Van et al. Optimizing the front side metallization procems using the corescan [J]. Conference record of the twenty-ninth IEEE photovoltaic specialists conference,2002, 340-3.

[3] T. Trupke, R.A. Bardos, M. Abbott, et al. Progress with luminescence imaging for the characterisation of silicon wafers and solar cells [J]. 2007.

[4] Karsten Bothe P, Jan Schmidt. Electrolumines ceflce imaging as an in-line characterizati On tool for solar cell production [J]. Record of the 21st European Photovoltaic Solar, 2006, 597-660.

[5] AY Liu. Research on weak boundary defect detection technology of solar cells based on deep learning [D]; Wuhan University of Science and Technology, 2021.

[6] XJ Tian. Research on silicon wafer crack detection algorithm based on optimized YOLOv3 neural network [D]; North University of China, 2019.

[7] DX Wang. Research on multi-target detection and tracking method based on deep learning. Dalian University of Technology [J]. 2021,

[8] Misra D. Mish: A Self Regularized Non-Monotonic Neural Activation Function [M]. 2019.

[9] Buerhop-Lutz C, Winkler T, Fecher F W, et al. Performance Analysis of Pre-Cracked PV-Modules at Realistic Loading Conditions; proceedings of the 33rd EUPVSEC, F, 2017 [C].